INTERFACE

royalsocietypublishing.org/journal/rsif

Research

Cite this article: Blamires SJ, Cerexhe G, White TE, Herberstein ME, Kasumovic MM. 2019 Spider silk colour covaries with thermal properties but not protein structure. *J. R. Soc. Interface* **16**: 20190199.
http://dx.doi.org/10.1098/rsif.2019.0199

Received: 21 March 2019
Accepted: 2 July 2019

Subject Category:
Life Sciences–Physics interface

Subject Areas:
biomimetics, biophysics, evolution

Keywords:
coloration, differential scanning calorimetry, major ampullate silk, optical models, spectrophotometry, wide-angle X-ray diffraction

Author for correspondence:
Sean J. Blamires
e-mail: sean.blamires@unsw.edu.au

Electronic supplementary material is available online at https://dx.doi.org/10.6084/m9.figshare.c.4573301.

THE ROYAL SOCIETY PUBLISHING

Spider silk colour covaries with thermal properties but not protein structure

Sean J. Blamires[1,2], Georgia Cerexhe[1], Thomas E. White[2,3], Marie E. Herberstein[2] and Michael M. Kasumovic[1]

[1]Evolution and Ecology Research Centre, School of Biological, Earth and Environmental Sciences E26, The University of New South Wales, Sydney 2052, Australia
[2]Department of Biological Science, Macquarie University, Sydney, New South Wales 2109, Australia
[3]School of Life and Environmental Sciences, Macleay (A12), Room 208, The University of Sydney, Sydney, New South Wales 2006, Australia

SJB, 0000-0001-5953-3723; TEW, 0000-0002-3976-1734; MMK, 0000-0003-0158-5517

Understanding how and why animal secretions vary in property has important biomimetic implications as desirable properties might covary. Spider major ampullate (MA) silk, for instance, is a secretion earmarked for biomimetic applications, but many of its properties vary among and between species across environments. Here, we tested the hypothesis that MA silk colour, protein structure and thermal properties covary when protein uptake is manipulated in the spider *Trichonephila plumipes*. We collected silk from adult female spiders maintained on a protein-fed or protein-deprived diet. Based on spectrophotometric quantifications, we classified half the silks as 'bee visible' and the other half 'bee invisible'. Wide angle X-ray diffraction and differential scanning calorimetry were then used to assess the silk's protein structure and thermal properties, respectively. We found that although protein structures and thermal properties varied across our treatments only the thermal properties covaried with colour. This ultimately suggests that protein structure alone is not responsible for MA silk thermal properties, nor does it affect silk colours. We speculate that similar ecological factors act on silk colour and thermal properties, which should be uncovered to inform biomimetic programmes.

1. Introduction

Biomimetics is an emergent scientific endeavour wherein researchers explore the properties of natural phenomena as inspiration for new synthetic designs and developments [1]. For instance, the mechanisms enabling animals to vary the colour of secretions such as hair, feathers, mucous and silk over time or across environments intrigues biomimetics research as the underlying principles inspire the development of innovative new coloured materials [2–6]. Likewise, the thermal properties of animal secretions may inspire the creation of new heat and light sensing materials [7].

Spider major ampullate (MA) silk is considered one of nature's toughest materials [8]. It thus comes as no surprise that many researchers have attempted to understand the intricacies of its structure–function relationship with a vision to create silk biomimetic products for medical and engineering applications (see reviews by Blamires *et al*. [8], Eisoldt *et al*. [9], Hsia *et al*. [10] and Ebrahimi *et al*. [11]). Consequently, we know that MA silk is hierarchically organized with a lipid, protein and glycoprotein-rich skin around a fibrous outer and inner core [8,12,13]. The silk core is traditionally thought to be composed of two proteins called spidroins: MA spidroin 1, or MaSp1, and MA spidroin 2, or MaSp2 (but see Babb *et al*. [14] and Correa-Garhwal *et al*. [15] for the potential inclusion of additional spidroins). MaSp1 consists of repeating polyalanine, $(GA)_n$, $(GGX)_n$ and $(A)_n$ amino acid motifs (G = glycine, A = alanine and X = other amino acids) that are expected to combine to promote the formation of β-sheet secondary structures in the assembled fibres [16,17]. The MaSp2 protein on the other hand is

thought to consist of additional multiple $(GPGXX)_n$ motifs (where P = proline) and has been predicted to form the so-called 'amorphous region', consisting of disordered type II β-turns and other secondary structures [18,19]. These secondary structures form a range of crystalline and amorphous protein tertiary structures, which have been considered the basis for spider silk's remarkable mechanical performance [8,13,20].

In addition to its impressive mechanical properties, spider MA silk has inimitable optical and thermal properties [21–23]. Understanding silk optical properties may inspire biomimetic applications such as the development of new highly efficient lenses, sensors or optic fibres [24–26]. It thus provides for a fruitful line of research. We know that MA silk has a high refractive index despite being largely translucent [21,22,27], which explains why it is visible to the naked human eye even though it is exceptionally thin (diameter: approx. 1–5 µm). We also know that the visibility, coloration and brightness of MA silk varies across environments, both among spider species and between individuals [28–31].

The skin, which primarily functions to prevent fibre biodegradation [32], is consistently smooth and homogeneous across species and individuals [33,34] so surface features are unlikely to induce inter- or intraspecific variation in coloration. Why MA silk should vary in colour among and between species and individuals is thus unknown. Nevertheless, there are some potential explanations. First, the shape and thickness of the skin, the appearance of cracks or microfibrils, twisting and accumulation of particulate debris may affect some of the silk's optical properties [26,35,36]. Second, pigments and other compounds, such as phenols, porphyrins, quinones and carotenoids, may reside within the skin layer and are thought to be responsible for some of the species-specific silk coloration variation [6,30,37,38]. Third, the β-sheet secondary structures and crystalline tertiary structures of MA silk are anisotropic, thus highly birefringent [39,40]. Given that the size, density and alignment of β-sheets can vary across spider species [41], this may contribute to variation in MA silk optical properties across species. Fourth and finally, the thermal properties of MA silk, particularly the silk's enthalpy (a measure of the total internal energy in the silk thread), glass transition temperature (T_g) and melt temperature, are hypothesized to covary with the size and alignment of the silk's crystalline structures and, thus, correlate with its birefringent properties [42,43]. The interactions between thermal properties and protein structure are observably manifested upon exposure to water as a downward shift in T_g due to changes in structural alignment [44].

While it might be deduced that there should be evolutionary and ecological consequences for environmentally induced variation in silk coloration across species and/or individuals, it is not readily apparent what these may be. It has been deduced that more colourful or visible silks might alert prey to the presence of the web or predators to the presence of the spider [45]. Accordingly, MA silk should always be inconspicuous against its background for the spider to effectively capture prey and avoid predators. In some instances, nonetheless, MA silk seems to reflect light at wavelengths selectively attractive to certain prey insects [28,46,47]. The consequent fitness benefit of such selective visibility is greater prey capture success, which may provide an evolutionary explanation for the conspicuous yellow (to the human eye) coloration of the silks of *Nephila* or *Trichonephila* spp. [29].

Here, we investigated how a spider's diet relates to silk colour and the underlying structural mechanisms and covarying properties. We know that the protein composition of the spider's diet can, to a certain extent, influence spider silk coloration [48]. Whether this is a product of a change in pigment deposition as different nutrients are made available, or a consequence of changes in birefringence accompanying the changes in protein structural properties associated with such dietary shifts [41,49] are unknown. If variation in silk colour is a consequence of changes to protein structures, then both the structures responsible and thermal properties should covary with coloration across diets. We accordingly tested our prediction by quantifying MA silk coloration (as spectral reflectance functions), crystalline secondary structures and thermal properties in the spider *Trichonephila plumipes* (formerly *Nephila plumipes*, see Kuntner *et al*. [50] for nomenclature).

2. Material and methods

2.1. Spiders

We used adult female *T. plumipes* collected from suburban Sydney, Australia for the following experiments. We measured their body length and width to ±0.1 mm using digital Vernier calipers (Caliper Technologies Corp., Mountain View, CA, USA) and mass to ±0.001 g using an electronic balance (Ohaus Corp., Pine Brook, NY, USA). Using these data, we took 30 individuals of similar mass that appeared not to be gravid to the laboratory at the University of New South Wales, Sydney, for the following procedures.

2.2. Experimental feeding regimes

Spiders were initially placed in 115 mm (wide) × 45 mm (high) plastic circular containers with perforated wire mesh lids, as described by Blamires *et al*. [41,48,49], and fed a 30% weight per volume concentration (w/v) glucose solution daily over 5 days. This feeding regime ensured that all influences of recent diet on protein structure or silk coloration were minimized [48]. We reweighed all of the spiders after the fifth day of feeding and removed one individual that lost excessive mass after constructing an eggsac. The remaining spiders were randomly allocated into two treatments: protein-fed (P) or protein-deprived (N).

The solution used for the protein-fed treatment was identical to that described by Blamires *et al*. [41,49]: a mixture of 10 g of a 10% albumin solution with 6 g of sucrose in 60 ml of water. The solution for the protein-deprived treatment was 8 g of sucrose in 30 ml of water. We fed the spiders the solutions by placing a 20 µl droplet onto their chelicerae using a micropipette. The spiders were fed the respective treatments over 10 days. After completing the experiment, we re-weighed all of the spiders and excluded any that lost excessive mass and/or built an eggsac (i.e. one from each treatment).

The above experiment was performed under controlled temperature (approx. 25°C) and humidity (approx. 50% RH) in still air.

2.3. Silk collection

Upon completing the feeding experiments, we collected MA silk from all of the 26 remaining spiders (13 per treatment) for spectrophotometry, wide-angle X-ray diffraction (WAXS) and differential scanning calorimetry (DSC) analyses as follows. We firstly anaesthetized all of the spiders using carbon dioxide and placed them ventral side up on a foam platform and immobilized them using non-adhesive tape and pins. We then carefully collected a single MA silk thread from the spinnerets. This procedure was performed under a dissecting microscope to ensure that a single thread from one spinneret was collected. An electronic spool rotating at

1 m min^{-1} was used to reel silk threads from each spider by two different collection methods.

First, to collect the silk for both spectrophotometry and WAXS a single MA silk thread was pulled across 3 mm × 1 mm titanium frames containing 0.5 mm × 0.5 mm windows. We then spooled the silk for 1 h, which resulted in approximately 1000 rounds being collected across the frame windows (see Benamú *et al*. [51] for details). Second, the silk was wrapped around a glass tube connected to the rotating spool for another 1 h. This resulted in approximately 15 mg of thread being wound onto the glass tube. The thread was scraped off the tube using a scalpel and bundled and placed into a 2 ml Eppendorf tube.

2.4. Spectrophotometry

We measured the reflectance spectra over the 300–700 nm waveband for the frame mounted silks using a Jaz spectrophotometer (Ocean Optics Inc., Largo FL, USA). We used the frame mounted silks for this process as each of the rounds of thread were in parallel, thus thread orientation could not interfere with our spectrophotometric measurements. The spectrophotometer was connected to a QR200-7UV-VIS reflection probe, held perpendicular to the sample, and a laptop running the program OceanView 1.6.3 (Ocean Optics, Inc.) via a series of SMA 905 optical fibres (to 0.22 numerical aperture), a reading fibre and a halogen light source (DT-1000, Ocean Optics, Inc.). Labsphere certified white (SRS-99-010) and black (SRS-02-010) reflectance standards [52] were used to calibrate the spectrometer to 100% and 0% reflectance, respectively. The area captured in all instances was 2 mm^2, and the integration time was 150 ms. Three repeated measurements for each silk bundle and the standards were taken in a dark room against a black cardboard background (corroborated against the Labsphere black standard). We subsequently plotted reflectance curves representing an average of the three repeated measurements per individual spider.

To interpret the reflectance spectra attained for the silks in a biologically relevant context (i.e. how they were viewed by prey), we performed visual models to ascertain whether any of the silks produced were viewed differently by honeybees, a common prey for *T. plumipes* in Sydney. We accordingly calculated the relative quantum flux absorbed by honeybee photoreceptors (P) across the 300–700 nm waveband using the following equation:

$$P = R\int_{300}^{700} I_S(\lambda)S(\lambda)D(\lambda)\mathrm{d}\lambda, \tag{2.1}$$

where $I_S(\lambda)$ is the spectral reflectance function of the silk, $S(\lambda)$ is the combined spectral sensitivity function of the six photoreceptors within a honeybee ommatidium [53], and $D(\lambda)$ is the daylight spectrum (CIE Standard Illuminant D65 [54]). The sensitivity factor (R) is determined by the following equation:

$$R = \frac{1}{\int_{300}^{700} I_B(\lambda)S(\lambda)D(\lambda)\,\mathrm{d}\lambda}, \tag{2.2}$$

where $I_B(\lambda)$ is the spectral reflection function of a typical vegetation background ascertained according to Blamires *et al*. [55]. We assumed that the honeybee photoreceptors were adapted to background coloration and that the photoreceptors displayed half their maximum response at all times.

The excitation (E) index of honeybee UV, blue and green photoreceptors while viewing each silk against a green background were subsequently estimated from their quantum flux values (P), using the equation below, derived from the colour hexagon model of Chittka [56]:

$$E = \frac{P}{P+1}. \tag{2.3}$$

We also estimated the discriminability of the silks by a honeybee viewer using the receptor-noise limited model, assuming a Weber fraction of 0.13, log-transformed quantum catches and a relative UV: blue: green receptor density of 1: 0.47: 4.41 [57,58]. Our results were qualitatively unchanged from those detailed below for the hexagon model, with 'white' silks estimated to be indiscriminable ($t_{10} = -1.25$, $p = 0.881$) and 'yellow' silks discriminable ($t_{13} = 2.34$, $p = <0.001$) considering a threshold of one just noticeable distance. Estimated colour-distances were also highly correlated between hexagon and receptor-noise models ($r = 0.98$). We thus refer to the results of the hexagon model henceforth, since it represents the most rigorously validated model for honeybee viewers [56,59]. We performed the visual models using the R package 'pavo' v. 2.2 [60].

2.5. Wide-angle X-ray diffraction analysis

WAXS provides detailed information on silk protein structures across secondary and tertiary levels. We accordingly measured the size, density and orientation of the crystalline and amorphous structures of the frame-mounted silks using WAXS at the SAXS/WAXS beamline at Australian Synchrotron, Melbourne, Australia. We taped each of the silk-containing frames to a sample plate supplied by the Centre. The plates were mounted onto a holdfast a distance of 330 mm away from the incident X-ray beam. The beam size was confined by a collimator 0.5 mm in diameter. A digital camera was set up enabling us to move the specimens into the beam line from outside the experimental hutch. We exposed each silk sample to the beam for 10–60 s depending on its density. The radiation scattered from each sample was detected by a Mar 165 imaging plate over a Q range of approximately 1.45 Å. Two-dimensional WAXS images were developed using the program Scatterbrain (Australian Synchrotron, Melbourne, Australia), from which the: (i) scattering parameter (q), (ii) diffraction angles (2θ), (iii) azimuthal angles, (iv) intensity peaks (I_x) and (v) full width and half width maximum intensities of the 2θ and azimuthal angles were calculated. These parameters allowed us to thereupon calculate: (i) d-spacing (or relative distances between pleated β-sheet) among the crystalline structures, (ii) relative crystalline intensity ratios ($I_{020}/I_{\mathrm{amorphous}}$ and $I_{210}/I_{\mathrm{amorphous}}$) with I_{020}, I_{210} and $I_{\mathrm{amorphous}}$, representing the sum of the scattering intensity at the (0 2 0) and (2 1 0) Bragg reflections and the amorphous halo, respectively, (iii) crystallinity index (X_c), representing an estimate of size of β-sheet crystallites and (iv) Herman's orientation function (f_c). Details pertaining to the application, analytical procedures and equations used in the WAXS analyses are found elsewhere [41,49,51].

2.6. Differential scanning calorimetry

DSC detects the heat flow into or out of biological polymeric materials, such as silks undergoing phase transitions [61,62]. It has thus been used to measure the enthalpy, degradation, crystallization, melt temperatures and T_g of silks (see [62–64] and the electronic supplementary material). While not a direct measure of protein structure, it has been used by some researchers to infer protein secondary and tertiary structures in silk [63–65]. We nevertheless used DSC herein to determine the parameters: (i) melt temperature, (ii) T_g and (iii) total internal enthalpy of the silks collected on glass tubes. The full procedures are outlined in the electronic supplementary material.

Each silk sample was placed individually within Tzero aluminium DSC pans with hermetic lids sealed with a Tzero press (TA Instruments, Austin, MN, USA) at the Centre for Advanced Macromolecular Design (CAMD), Faculty of Engineering, University of New South Wales. Conventional mode DSC was performed using a Q20 differential scanning calorimeter (TA Instruments, Austin, MN, USA). The rate of heating was set to 3°C min^{-1} over the −50 to +200°C temperature range and modulation amplitude

was set at 1°C with a period of 60 s. A blank pan (i.e. one without a sample added) was prepared as a reference and simultaneously added to the calorimeter along with the sample pans. We thereupon estimated T_g, melt temperature and enthalpy, as described in the electronic supplementary material.

2.7. Statistical analyses

We used one sample *t*-tests to compare the colour contrast values, calculated in hexagon units, as the Euclidean distances between the summed excitation indices for the calculated honeybee UV, blue and green photoreceptors over colour space, with a discrimination threshold value of 0.10, i.e. we assumed differentially conditioned bees to always view the silks [59,66]. We also calculated the contrasts between the green photoreceptor excitation values and the vegetation background to estimate the achromatic contrast values and compared them with the 0.10 discrimination threshold [67,68]. Where an individual silk exceeded the chromatic or achromatic discrimination threshold we considered them to be 'bee visible', whereas those that did not exceed any of the discrimination thresholds were considered 'bee invisible'.

We used discriminant function and least significant difference *post hoc* analyses to determine whether the: (i) *d*-spacing, crystalline intensity ratios, crystallinity indices and/or Herman's orientation functions and (ii) degradation temperature, T_g, and enthalpy varied between the protein-fed and protein-deprived treatments. We used a categorical Pearson's χ^2-test to ascertain whether the proportion of silks that we classified as bee visible and bee invisible differed across treatments. Prior to performing these analyses we checked the data for normality, linearity and homoscedasticity using quantile–quantile and probability plots.

To determine whether changes to silk protein structures and thermal properties covaried with silk coloration across diets we plotted redundancy analysis (RDA) ordinations [69] of protein structures and thermal properties against silk visibility (classified as bee visible or bee invisible as explained above). The individual WAXS and DSC parameters were collapsed to first redundancy variables for the RDA. Where ordinations showed across parameter differentiation between the bee visible and bee invisible silks we interpreted this as indicating that silk coloration was associated with its protein structures and/or thermal properties.

3. Results

The spectral reflectance functions for the MA silks of all individual spiders were highly variable across both of the treatments (figure 1). The mean chromatic and achromatic contrast of silks from each of the feeding treatments fell below the detection threshold for ($\chi^2_{23} = 0.110$; $p = 0.597$; see mean values in figure 2*a*,*b*). Nevertheless upon closer examining the data points in figure 2, it is evident that approximately half of all silks (i.e. 14 of 26) could be classifiable as bee visible and the others (12 of 26) could be classifiable as bee invisible based on their absolute colour contrast values, independent of the treatment (see data points in figure 2*a*,*b*). Representative reflectance spectra for each of these silks are shown in figure 3*a*. The silks that were classified as bee visible appeared yellow or golden to the naked human eye, while those classified as bee invisible appeared white to silver to the naked eye (figure 3*b*).

Our discriminant function analyses revealed that the WAXS derived *d*-spacing, $I_{210}/I_{amorphous}$ and Herman's orientation functions differed between the silks of the protein-deprived and protein-fed spiders (tables 1 and 2), as did the DSC derived degradation temperature, T_g, and enthalpy (tables 3 and 4;

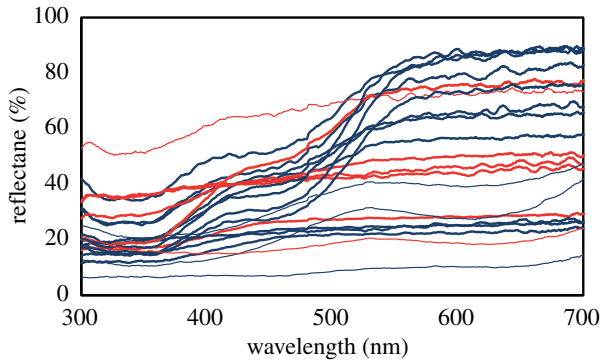

Figure 1. Reflectance spectra of the silks from the P-treatment spiders (blue curves) and N-treatment (red curves) spiders. (Online version in colour.)

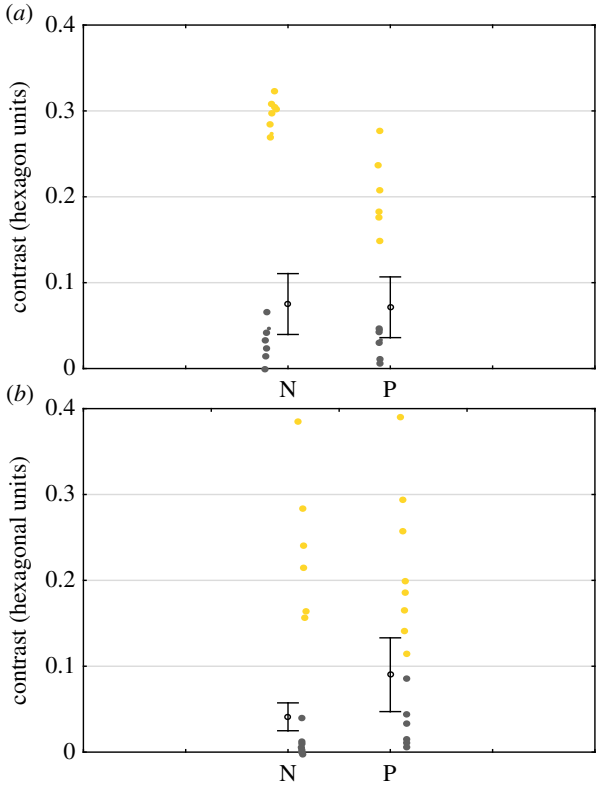

Figure 2. Scatter and means-error plots of chromatic (*a*) and achromatic (*b*) contrast values of silks from both N and P treatments. Yellow data points of the scatter plots represent measurements for each silk classified as bee visible and the silver data points represent those for silks classified as bee invisible. Dots in the means-error plots represent mean values and the whiskers represent ±1 s.e. The dotted line at 0.10 in each plot shows the threshold value for classification as bee visible. The coloured dots in the figure refer to the colours of each silk as seen by the human eye. (Online version in colour.)

see also electronic supplementary material, figures S1 and S2, respectively, for WAXS images and heat flow versus temperature thermographs across treatments).

Our RDA ordinations nevertheless showed that while silk colour explained approximately 53% of the variance in protein structures, it was not associated with any of the structural parameters we measured using WAXS (figure 4*a*). On the other hand, silk colour explained approximately 95% of the thermal property variance, and our ordinations (figure 4*b*) and the DSC thermographs (electronic supplementary material, figure S3) showed that the degradation temperature

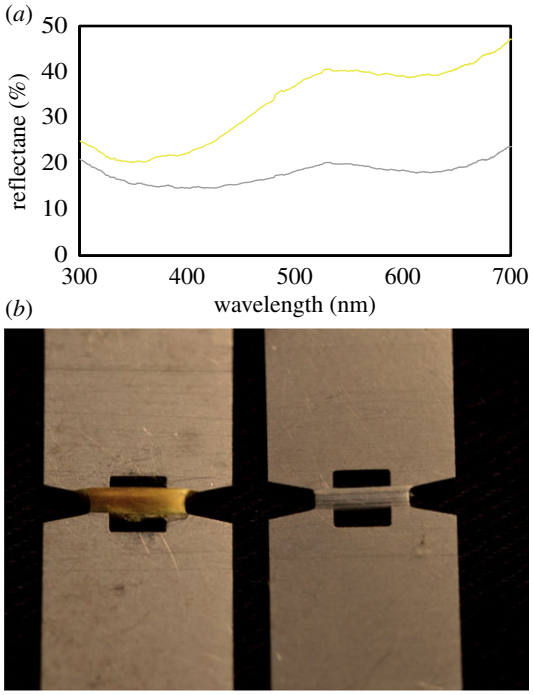

Figure 3. (*a*) Reflectance spectra of the bee visible silks (yellow line) and bee invisible silks (silver line). (*b*) Examples of bee visible silk (the yellow/golden silk on the left) and bee invisible silk (the white/silver silk on the left) as they appeared to the human eye when wound around the titanium frames in preparation for spectrophotometry and WAXS. (Online version in colour.)

and T_g of the bee visible silks were distinctly different from those of the bee invisible silks.

4. Discussion

We deprived the spider *Trichonephila plumipes* of protein, and performed spectrophotometry, WAXS and DSC analyses on its MA silks to investigate whether the changes in silk protein structures and/or thermal properties were associated with any changes in silk coloration. We found that while the protein structures and thermal properties varied between treatments, only the thermal properties were associated with silk colour, and that this association occurred irrespective of protein intake. We thus suggest that protein structures alone are not responsible for MA silk thermal properties and they do not drive silk colour.

About half of all of the silks we examined across both treatments could be classified as bee visible and the other were classifiable as bee invisible. Moreover, the bee visible silks always appeared yellow/golden to the human eye, while the bee invisible silks always appeared white/silver to the human eye. We would like to note that in the field we almost always observe spiders in webs comprised of yellow silk. Nevertheless, the fact that we had substantial colour variation in the silks collected in the laboratory (yellow to white) allowed us to compare the characteristics of the different coloured silks more closely and make two broad conclusions about the colour of *T. plumipes* silk. Firstly, the yellow and white colours are not related to the spider's protein intake, at least under the regimes tested herein. Secondly, silk thermal properties but not protein structure correlated with silk colour. The ecological implications for silk coloration variation across species/individuals are not known, partly because the colour variation remains, until now, unquantified. Hence our findings provide valuable insights into the mechanisms and consequences of silk coloration variation.

Our results suggest that changes in silk protein structures do not affect silk colour via variation in the silk's refractivity or birefringence. We thus expect the most likely cause of the yellow or white coloration observed in *T. plumipes* silk to be pigment deposition, as has been speculated for *Trichonephila clavipes* [6,37]. We do not currently know which pigments are present in *T. plumipes* MA silks. Putthanarat *et al*. [37] speculated that depositions of hydroxylated benzoquinone, naphthaquinone and other quinones within the silk skin are responsible for the yellow coloration in *T. clavipes* silks. Hsiung *et al*. [6] on the other hand found evidence that β-carotene deposition was responsible for yellow coloration in *Nephila pilipes* MA silk.

Various carotenoids induce orange and yellow coloration in moth cocoon silks [70–73]. Since spiders cannot synthesize β-carotene de novo, the pigments need to be taken up via the spider's diet [6,73]. Our finding that half of the silks we retrieved were yellow irrespective of protein intake suggested that the yellow coloration of *T. plumipes* silk is unlikely to be due to carotinoid intake and deposition within the silk skin. We nonetheless occasionally noticed that the yellow-coloured silk became white toward the end of silk collecting, suggesting that the spiders might have been depleted of a pigment, or other colour inducing compound after approximately 2 h of being forcibly silked. Ongoing analyses using nuclear magnetic resonance, Fourier transform infrared spectroscopy and pigment transcript analyses should, in time, confirm which pigments, if any, induce the yellow/golden colour of *T. plumipes* MA silks.

An examination of figure 1 shows a more marked modulation at approximately 470–500 nm, i.e. within the blue to green region, in the reflectance spectra of the silks of spiders from the protein-fed treatment (blue curves) compared to those of spiders from the protein-deprived treatment (red curves). The modulations were however not manifested, as both of our visual models found that the protein-fed treatment spider silks were not any more discriminable by honeybees than the protein-deprived treatment spider silks. This was likely a consequence of the green background against which the silks were contrasted also having a modulation in the green region of the spectrum. We cannot say from examining reflectance spectra alone whether these modulations indicate the presence of pigments, such as porphyrins, variation within the surface or structural features, or are an anomaly. We nevertheless expect that the presence of a pigment is unlikely because porphyrin, or another other green pigment, would need to be consumed in order to be expressed in silk [74].

The protein structural properties, particularly the orientation and alignment of crystalline and amorphous secondary structures, are thought to influence the thermal properties of MA silk [36,63,75]. This likely explains why both protein structures and thermal properties varied between our feeding treatments. Nevertheless, a lack of any significant association between *T. plumipes* silk's protein structures, thermal properties and coloration suggests that factors other than protein structures are affecting the thermal properties and coloration. We do not know why the thermal properties and coloration of *T. plumipes* MA silk covaried independent of

Table 1. Results of a discriminant function and least significant difference *post hoc* analyses determining whether silk crystal sizes, crystalline intensity ratios, crystallinity indices and Herman's orientation functions varied between the four species. Comparisons of means (±1 s.e.) across treatments. Significance of *p*-values is indicated by asterisk.

	d-spacing (nm)	$I_{020}/I_{amorphous}$	$I_{210}/I_{amorphous}$	crystallinity index	Herman's orientation
P-treatment	0.710 ± 0.161	1.223 ± 0.005	1.011 ± 0.030	1.342 ± 0.048	0.235 ± 0.205
N-treatment	0.592 ± 0.092	1.222 ± 0.004	1.059 ± 0.018	1.375 ± 0.072	0.132 ± 0.102
Wilk's lambda	0.101	0.088	0.141	0.091	0.138
partial lambda	0.738	0.897	0.561	0.867	0.572
F-remove (d.f. = 1,24)	3.598	1.481	10.577	1.983	9.692
p-value	0.021*	0.234	<0.001*	0.132	<0.001*
tolerance	0.792	0.269	0.238	0.672	0.584
1-tolerance	0.208	0.731	0.762	0.328	0.416

*$p < 0.05$.

Table 2. Results of a discriminant function and least significant difference *post hoc* analyses determining whether silk crystal sizes, crystalline intensity ratios, crystallinity indices and Herman's orientation functions varied between the four species. Raw coefficients of the canonical variables.

roots removed	eigenvalue	canonical R	Wilk's lambda	χ^2	d.f.	*p*-value
0	3.567	0.883	0.079	105.093	15	<0.001
1	1.719	0.795	0.363	42.052	8	<0.001
2	0.012	0.113	0.987	0.534	3	0.911

Table 3. Results of a discriminant function and least significant difference *post hoc* analyses to determine whether melt temperature, glass transition temperature and enthalpy varied between the four species. Comparisons of means (±1 s.e.) across the four species. Significance of *p*-values is indicated by asterisk.

	melt temperature (°C)	glass transition temperature (°C)	enthalpy (J g^{-1})
P-treatment	193.56 ± 4.36	147.93 ± 1.64	229.54 ± 94.80
N-treatment	196.28 ± 3.55	152.34 ± 1.11	258.10 ± 86.81
Wilk's lambda	0.006	0.001	0.007
partial lambda	0.252	0.143	0.229
F-remove (d.f. = 1,24)	43.913	79.433	45.921
p-value	<0.001*	<0.001*	<0.001*
tolerance	0.821	0.917	0.884
1-tolerance	0.179	0.083	0.116

*$p < 0.05$.

Table 4. Results of a discriminant function and least significant difference *post hoc* analyses to determine whether melt temperature, glass transition temperature and enthalpy varied between the four species. Raw coefficients of the canonical variables.

roots removed	eigenvalue	canonical R	Wilk's lambda	χ^2	d.f.	*p*-value
0	373.879	0.998	<0.001	369.192	9	<0.001
1	12.941	0.963	0.063	117.311	4	<0.001
2	0.1336	0.343	0.882	5.329	1	0.021

protein structures, but we suspect a combination of changes within the structural integrity and composition of the skin, including any pigment deposition, to be responsible.

Water infiltrates hydrogen bonds between amorphous region proteins in MA silk, causing the crystalline and amorphous region proteins to become misaligned along the fibre's axis

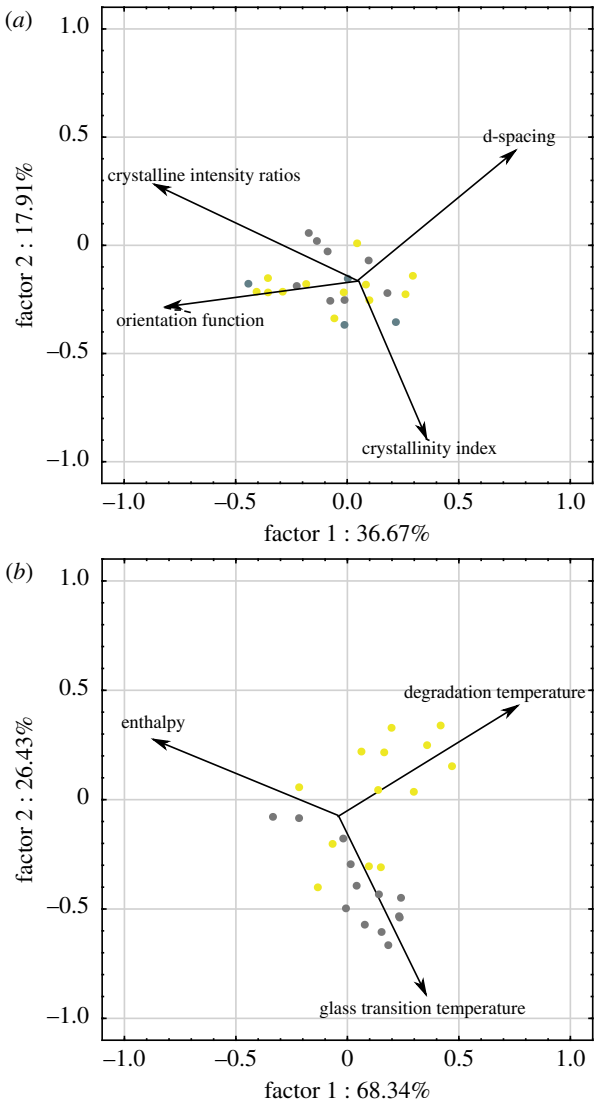

Figure 4. RDA ordinations of the association between the variance in silk colour and variance in (*a*) structural parameters measured using WAXS and (*b*) thermal property parameters measured using DSC. (Online version in colour.)

without changes in density [76,77]. A change in crystalline alignment alone may be enough to significantly shift T_g so the silk becomes rubbery at room temperature (20–30°C) [36,38,76,77]. Water is therefore an agent that may simultaneously affect MA silk thermal properties and protein structure. However, our experiments were performed under controlled temperature (approx. 25°C) and humidity (approx. 50% RH) conditions so water infiltration probably had a minor effect on the protein structures and/or thermal properties measured herein. It might nonetheless explain why we calculated slightly lower T_g values than that deduced for other spider silks.

We found differences in the thermal properties of *T. plumipes* silks between treatments and among the different coloured silks as a consequence of significant variation in heat flow across treatments and the different coloured silks. An examination of our DSC thermographs revealed that there were no major shifts in topography between treatments or across the different coloured silks (i.e. they always showed an endothermic response across the temperature range), and T_g was consistent at approximately 140–150°C, with melt temperature peaks always observed at greater than 160°C, and thermal degradation consistently commenced at around 180–200°C (see electronic supplementary material, figures S2 and S3). These values approximate the ranges reported for other MA silks [63,75], with the exception of T_g which was marginally lower. We also found that silk crystallinity did not vary greatly between feeding treatments, or among the different coloured silks. It seems therefore evident that there was no major phase transition or crystalline region breakdown across treatments or among the different coloured silks, ruling out further water infiltration as a cause of thermal property differences across the bee visible and bee invisible silks.

An additional possibility is that the two distinct silk colours that we identified (bee visible and bee invisible) are unique to the assumed honeybee viewer which, while appropriate given our knowledge of prey composition for our focal spiders, does not capture the full diversity of potential viewers nor viewing conditions. Furthermore, we measured the spectra of silks herein by wrapping them tightly around metal cards, meaning the silks appeared different from what would be expected in a web, where they are distributed more sparsely and orientated in a multitude of different directions. With that said, the models used and sample preparations also might affect the colour classifications of the silk based on its visibility to different insects. More testing is clearly required to ascertain the visibilities of the silks to different prey or predators. Notwithstanding, there are difficulties ascribing an ecological function to any estimated colour classifications because the light weight, translucency and exceptional thinness of silks render them extremely difficult to discern by insects under field conditions.

A further possibility that our findings suggest is that the different silk colours might be more associated with the regulation of silk thermal properties than any perceptual ecological advantages, such as attracting prey [28,46,47]. Perhaps subtle changes to skin size or composition (e.g. by the deposition of pigments), or appearance (e.g. by twisting), ensures that the silk proteins do not undergo unintended denaturation as temperature and/or humidity changes over time. Conversely, silk coloration may be selected for as a mechanism for attracting prey under certain conditions and any subsequent changes in thermal properties are an unavoidable artefact. Regardless of the evolutionary or ecological consequences and mechanisms, there are likely to be trade-offs between prey/predator attraction and avoidance as consequences of enhanced/reduced silk visibility and thermal properties as spider diets vary over time and/or space. It is the balance of this trade-off that likely determines whether *T. plumipes* silks appear visible or invisible to bees in any environment. We have seen other spiders using similar yellow-coloured silks when they build their webs in similar open habitats to those exploited by *T. plumipes* (see the electronic supplementary material, figure S4 for an example), suggesting that other spiders may vary their silk coloration in a similar way across diets or other ecological circumstance. Certainly, more comparative analyses of silk coloration, spider diets, web building, habitat preferences and the fitness benefits associated with the use of different coloured silks are warranted to test these hypotheses.

A broader implication of our findings is that they suggest that it is possible to develop biomimetic silk-like fibres with variable protein structures, hence variable mechanical properties, while holding the optical properties constant and vice versa. Nevertheless, thermal properties might inadvertently covary with optical properties. We thus recommend further research focus on the mechanism of this covariation so we can ascertain how to go about disentangling the covarying parameters during fibre construction.

Data accessibility. Data are accessible from Dryad.

Authors' contributions. S.J.B. designed the study and drafted the manuscript. G.C., T.E.W. and M.E.H performed the experiments, and carried out data analysis. S.J.B., M.E.H. and M.M.K. supplied materials. All authors gave final approval for publication.

Competing interests. We declare we have no competing interests.

Funding. S.J.B. was supported by Australian Research Council and Hermon Slade Foundation grants.

Acknowledgements. Elizabeth Lowe shared information about collection sites. Anthony Granville arranged access to DSC facilities at CAMD. Adrian Hawley assisted with WAXS analyses at Australian Synchrotron. Keiji Numata commented on an early version of the paper.

References

1. Wolff JO, Wells D, Reid C, Blamires SJ. 2017 Clarity of objectives and working principles enhances the success of biomimetic programs. *Bioinspir. Biomim.* **12**, 051001. (doi:10.1088/1748-3190/aa86ff)
2. Sharma V, Crne M, Park JO, Srinivasarao M. 2009 Structural origin of circularly polarized iridescence in jeweled beetles. *Science* **325**, 449–451. (doi:10.1126/science.1172051)
3. Forster JD *et al.* 2010 Biomimetic isotropic nanostructures for structural coloration. *Adv. Mater.* **22**, 2939–2944. (doi:10.1002/adma.200903693)
4. Kolle M, Salgard-Cunha PM, Scherer MRJ, Huang F, Vukusic P, Mahajan S, Baumberg JJ, Steiner U. 2010 Mimicking the colourful wing scale structure of the *Papilio blumei* butterfly. *Nat. Nanotechnol.* **5**, 511–515. (doi:10.1038/nnano.2010.101)
5. Noh H, Liew SF, Saranathan V, Mochrie SGJ, Prum RO, Dufresne ER, Cao H. 2010 How noniridescent colors are generated by quasi-ordered structures of bird feathers. *Adv. Mater.* **22**, 2871–2880. (doi:10.1002/adma.200903699)
6. Hsiung BK, Justyn NM, Blackledge TA, Shawkey MD. 2017 Spiders have rich pigmentary and structural colour palettes. *J. Exp. Biol.* **220**, 1975–1983. (doi:10.1242/jeb.156083)
7. Zhou H, Xu J, Zhang H, Wang D, Chen Z, Zhang D, Fan T. 2018 Bio-inspired photonic materials: prototypes and structural effects designs for applications in solar energy manipulation. *Adv. Mater.* **2018**, 1705309. (doi:10.1002/adfm.201705309)
8. Blamires SJ, Blackledge TA, Tso IM. 2017 Physicochemical property variation in spider silk: ecology, evolution, and synthetic production. *Annu. Rev. Entomol.* **62**, 443–460. (doi:10.1146/annurev-ento-031616-035615)
9. Eisoldt L, Smith A, Scheibel T. 2011 Decoding the secrets of spider silk. *Mater. Today* **14**, 80–86. (doi:10.1016/S1369-7021(11)70057-8)
10. Hsia Y, Gnesa E, Jeffrey Y, Tang S, Viera C 2011 Spider silk composites and applications. In *Metal, ceramic and polymeric composites for various uses* (ed. J Cuppoletti), pp. 303–324. London, UK: Intech.
11. Ebrahimi D, Tokareva O, Rim NG, Wong JY, Kaplan DL, Buehler MJ. 2015 Silk—its mysteries, how it is made, and how it is used. *ACS Biomater. Sci. Eng.* **1**, 864–876. (doi:10.1021/acsbiomaterials.5b00152)
12. Papadopoulos P, Salter J, Kremer F. 2009 Similarities in the structural organization of major and minor ampullate spider silk. *Macromol. Rapid Commun.* **30**, 851–857. (doi:10.1002/marc.200900018)
13. Heim M, Römer L, Scheibel T. 2010 Hierarchical structures made of proteins. The complex architecture of spider webs and their constituent silk proteins. *Chem. Soc. Rev.* **39**, 156–164. (doi:10.1039/B813273A)
14. Babb PL *et al.* 2017 The *Nephila clavipes* genome highlights the diversity of spider silk genes and their complex expression. *Nat. Genet.* **49**, 895–903. (doi:10.1038/ng.3852)
15. Correa-Garhwal SM, Chaw RC, Clarke TH, Ayoub NA, Hayashi CY. 2017 Silk gene expression of theridiid spiders: implications for male-specific silk use. *Zoology* **122**, 107–114. (doi:10.1016/j.zool.2017.04.003)
16. Xu M, Lewis RV. 1990 Structure of a protein superfiber: spider dragline silk. *Proc. Natl Acad. Sci. USA* **87**, 7120–7124. (doi:10.1073/pnas.87.18.7120)
17. Parkhe AD, Seeley SK, Gardner K, Thompson L, Lewis RV. 1997 Structural studies of spider silk proteins in the fiber. *J. Mol. Recognit.* **10**, 1–6. (doi:10.1002/(SICI)1099-1352(199701/02)10:1<1::AID-JMR338>3.0.CO;2-7)
18. Hinman MB, Lewis RV. 1992 Isolation of a clone encoding a second dragline silk fibroin: *Nephila clavipes* dragline silk is a two-protein fiber. *J. Biol. Chem.* **267**, 19 320–19 324. (doi:10.2210/pdb2cgm/pdb)
19. Shi X, Holland GP, Yarger JL. 2015 Molecular dynamics of spider dragline silk fiber investigated by ^{2}H MAS NMR. *Biomacromolecules* **16**, 852–859. (doi:10.1021/bm5017578)
20. Hayashi CY, Shipley NH, Lewis RV. 1999 Hypotheses that correlate the sequence, structure, and mechanical properties of spider silk proteins. *Int. J. Biol. Macromol.* **24**, 271–275. (doi:10.1016/S0141-8130(98)00089-0)
21. Little DJ, Kane DM. 2011 Image contrast immersion method for measuring refractive index applied to spider silks. *Opt. Express* **19**, 19 182–19 188. (doi:10.1364/OE.19.019182)
22. Monks JN, Yan B, Hawkins N, Vollrath F, Wang Z. 2016 Spider silk: mother nature's bio-superlens. *Nano Lett.* **16**, 5842–5845. (doi:10.1021/acs.nanolett.6b02641)
23. Shimanovich U *et al.* 2018 Biophotonics of native silk fibrils. *Macromol. Biosci.* **18**, 1700295. (doi:10.1002/mabi.201700295)
24. Omenetto FG, Kaplan DL. 2008 A new route for silk. *Nat. Photonics* **2**, 641–643. (doi:10.1038/nphoton.2008.207)
25. Huby N, Vie V, Renault A, Beufils S, Lefévre T, Pasquet-Mercia F, Pézelot M, Bêche M. 2013 Native spider silk as a biological optical fiber. *Appl. Phys. Lett.* **102**, 123702. (doi:10.1063/1.4798552)
26. Kujala S, Mannila A, Karvonen L, Kieu K, Sun Z. 2016 Natural silk as a photonics component: a study on its light guiding and nonlinear optical properties. *Sci. Rep.* **6**, 22358. (doi:10.1038/srep22358)
27. Karthikeyani R, Divya A, Mathavan T, Ashath RM, Benial AM, Muthuchelian K. 2017 Structural and optical studies on selected web spinning spider silks. *Spectrochim. Acta A: Mol. Biomol. Spectrosc.* **170**, 111–116. (doi:10.1016/j.saa.2016.06.044)
28. Craig CL, Bernard GD, Coddington JA. 1994 Evolutionary shifts in the spectral properties of spider silks. *Evolution* **48**, 287–296. (doi:10.1111/j.1558-5646.1994.tb01312.x)
29. Craig CL, Weber RS, Bernard GD. 1996 Evolution of predator-prey systems: spider foraging plasticity in response to the visual ecology of prey. *Am. Nat.* **147**, 205–229. (doi:10.1086/285847)
30. Pouchkina NN, Stanchev BS, McQueen-Mason SJ. 2003 From EST sequence to spider silk spinning: identification and molecular characterisation of *Nephila senegalensis* major ampullate gland peroxidase NsPox. *Insect Biochem. Mol. Biol.* **33**, 229–238. (doi:10.1016/S0965-1748(02)00207-2)
31. Lai CW, Zhang S, Piorkowski D, Liao CP, Tso IM. 2017 A trap and a lure: dual function of a nocturnal animal construction. *Anim. Behav.* **130**, 159–164. (doi:10.1016/j.anbehav.2017.06.016)
32. Yazawa K, Malay AD, Maunaga H, Numata K. 2019 Role of skin layers on mechanical properties and supercontraction of spider dragline silk fiber. *Macromol. Biosci.* **19**, 1800220. (doi:10.1002/mabi.201800220)
33. Li SFY, McGhie AJ, Tang SL. 1994 New internal structure of spider dragline silk revealed by atomic force microscopy. *Biophys. J.* **66**, 1209–1212. (doi:10.1016/S0006-3495(94)80903-8)
34. Kane DM, Naidoo N, Staib GR. 2010 Atomic force microscopy of orb-spider-web-silks to measure surface nanostructuring and evaluate silk fibers per strand. *J. Appl. Phys.* **108**, 073509. (doi:10.1063/1.3490220)
35. Augsten K, Muhlig P, Hermann C. 2000 Glycoproteins and skin-core structure in *Nephila clavipes* spider silk observed by light and electron microscopy. *Scanning* **22**, 12–15. (doi:10.1002/sca.4950220103)
36. Poza P, Pérez-Rigueiro J, Elices M, Llorca J. 2002 Fractographic analysis of silkworm and spider silk. *Eng. Fract. Mech.* **69**, 1035–1048. (doi:10.1016/S0013-7944(01)00120-5)
37. Putthanarat S, Zarbook S, Miller LD, Eby RK, Adams WW. 2004 The color of dragline silk produced in captivity by the spider *Nephila clavipes*. *Polymer* **45**, 1933–1937. (doi:10.1016/j.polymer.2004.01.020)

38. Guan J, Vollrath F, Porter D. 2011 Two mechanisms for supercontraction in *Nephila* spider dragline silk. *Biomacromolecules* **12**, 4030–4035. (doi:10.1021/bm201032v)
39. Carmichael S, Barghout JYJ, Viney C. 1999 The effect of post-spin drawing on spider silk microstructure: a birefringence model. *Int. J. Biol. Macromol.* **24**, 219–226. (doi:10.1016/S0141-8130(99)00008-2)
40. Little DJ, Kane DM. 2017 Investigating the transverse optical structure of spider silk micro-fibers using quantitative optical microscopy. *Nanophotonics* **6**, 341–348. (doi:10.1515/nanoph-2016-0125)
41. Blamires SJ, Nobbs M, Martens PJ, Tso IM, Chuang WS, Chang CK, Sheu HS. 2018 Multiscale mechanisms of nutritionally induced property variation in spider silks. *PLoS ONE* **13**, e0192005. (doi:10.1371/journal.pone.0192005)
42. Seydel T, Knoll W, Greving I, Dicko C, Koza MM, Krasnov I, Müller M. 2011 Increased molecular mobility in humid silk fibers under tensile stress. *Phys. Rev. E* **83**, 016104. (doi:10.1103/PhysRevE.83.016104)
43. Colomban P. 2013 Understanding the nano- and macromechanical behaviour, the failure and fatigue mechanisms of advanced and natural polymer fibres by Raman/IR microspectrometry. *Adv. Nat. Sci.* **4**, 013001. (doi:10.1088/2043-6262/4/1/013001)
44. Glisovic A, Vehoff T, Davies RJ. 2008 Strain dependent structural changes of spider dragline silk. *Macromolecules* **41**, 390–398. (doi:10.1021/ma070528p)
45. Bruce MJ, Heiling AM, Herberstein ME. 2005 Spider signals: are web decorations visible to birds and bees? *Biol. Lett.* **1**, 299–302. (doi:10.1098/rsbl.2005.0307)
46. Herberstein ME, Craig CL, Coddington JA, Elgar MA. 2000 The functional significance of silk decorations of orb-web spiders: a critical review of the empirical evidence. *Biol. Rev.* **75**, 649–669. (doi:10.1111/j.1469-185X.2000.tb00056.x)
47. Thery M, Casas J. 2009 The multiple disguises of spiders: web colour and decorations, body colour and movement. *Phil. Trans. R. Soc. B* **364**, 471–480. (doi:10.1098/rstb.2008.0212)
48. Blamires SJ, Sahni V, Dhinojwala A, Blackledge TA, Tso IM. 2014 Nutrient deprivation induces property variations in spider gluey silk. *PLoS ONE* **9**, e88487. (doi:10.1371/journal.pone.0088487)
49. Blamires SJ, Liao CP, Chang CK, Chuang YC, Wu CL, Blackledge TA, Sheu HS, Tso IM. 2015 Mechanical performance of spider silk is robust to nutrient-mediated changes in protein composition. *Biomacromolecules* **16**, 1218–1225. (doi:10.1021/acs.biomac.5b00006)
50. Kuntner M *et al.* 2019 Golden orbweavers ignore biological rules: phylogenomic and comparative analyses unravel a complex evolution of sexual size dimorphism. *Syst. Biol.* **68**, 555–572. (doi:10.1093/sysbio/syy082)
51. Benamú MA, Lacava M, Garcia LF, Santana M, Fang J, Wang X, Blamires SJ. 2017 Nanostructural and mechanical property changes to spider silk as a consequence of insecticide exposure. *Chemosphere* **181**, 241–249. (doi:10.1016/j.chemosphere.2017.04.079)
52. Labsphere Inc. 2017 *Spectralon® diffuse reflectance standards*. North Sutton, NH: Labsphere Inc.
53. Wakakuwa M, Kurasawa M, Giurfa M, Arikawa K. 2005 Spectral heterogeneity of honeybee ommatidia. *Naturwissenschaften* **92**, 464–467. (doi:10.1007/s00114-005-0018-5)
54. Malacara M. 2002 *Color vision and colorimetry: theory and applications*. Bellingham, WA: SPIE Press.
55. Blamires SJ, Hochuli DF, Thompson MB. 2008 Why cross the web? Decoration spectral properties and prey capture in an orb spider (*Argiope keyserlingi*) web. *Biol. J. Linn. Soc.* **94**, 221–229. (doi:10.1111/j.1095-8312.2008.00999.x)
56. Chittka L. 1992 The colour hexagon: a chromaticity diagram based on photoreceptor excitations as a generalized representation of colour opponency. *J. Comp. Physiol. A* **170**, 533–543. (doi:10.1007/bf00199331)
57. Vorobyev M, Osorio D. 1998 Receptor noise as a determinant of colour thresholds. *Proc. R. Soc. Lond. B* **265**, 351–358. (doi:10.1098/rspb.1998.0302)
58. Vorobyev M, Brant R, Peitsch D, Laughlin SB, Menzel R. 2001 Colour thresholds and receptor noise: behaviour and physiology compared. *Vis. Res.* **41**, 639–653. (doi:10.1016/S0042-6989(00)00288-1)
59. Dyer AG, Chittka L. 2004 Fine colour discrimination requires differential conditioning in bumblebees. *Naturwissenschaften* **91**, 224–227. (doi:10.1007/s00114-004-0508-x)
60. Maia R, Gruson H, Endler JA, White TE. 2019 pavo 2: new tools for the spectral and spatial analysis of colour in R. *Methods Ecol. Evol.* **10**, 1097–1107. *(*doi:10.1111/2041-210X.13174*)*
61. Gill P, Moghadam TT, Ranjbar B. 2010 Differential scanning calorimetry techniques: applications in biology and nanoscience. *J. Biomol. Tech.* **21**, 167–193.
62. Vollrath F, Hawkins N, Porter D, Holland C, Boulet-Audet M. 2015 Differential scanning fluorimetry provides high throughput data on silk protein transitions. *Sci. Rep.* **4**, 5625. (doi:10.1038/srep05625)
63. Hu X, Kaplan DL, Cebe P. 2006 Determining beta-sheet crystallinity in fibrous proteins by thermal analysis and infrared spectroscopy. *Macromolecules* **39**, 6161–6170. (doi:10.1021/ma0610109)
64. Guan J, Wang Y, Mortimer B, Holland C, Shao Z, Portr D, Vollrath F. 2016 Glass transitions in native silk fibres studied by dynamic mechanical thermal analysis. *Soft Matter* **12**, 5926–5936. (doi:10.1039/C6SM00019C)
65. McGill M, Holland GP, Kaplan DL. 2018 Experimental methods for characterizing the secondary structure and thermal properties of silk proteins. *Macromol. Rapid Commun.* **2018**, 1800390. (doi:10.1002/marc.201800390)
66. Blamires SJ, Hou C, Chen LF, Liao CP, Tso IM. 2014 A predator's body coloration enhances its foraging profitability by day and night. *Behav. Ecol. Sociobiol.* **68**, 1253–1260. (doi:10.1007/s00265-014-1736-5)
67. Srinivasan MV, Lehrer M. 1988 Spatial acuity of honeybee vision and its spectral properties. *J. Comp. Physiol. A* **162**, 159–172. (doi:10.1007/BF00606081)
68. Olsson P, Lind O, Kelber A. 2018 Chromatic and achromatic vision: parameter choice and limitations for reliable model predictions. *Behav. Ecol.* **29**, 273–282. (doi:10.1093/beheco/arx133)
69. Van den Wollenberg AL. 1977 Redundancy analysis: an alternative for canonical correlation analysis. *Psychometrika* **42**, 207–219. (doi:10.1007/BF02294050)
70. Sakudoh T *et al.* 2007 Carotenoid silk coloration is controlled by a carotenoid-binding protein, a product of the Yellow blood gene. *Proc. Natl Acad. Sci. USA* **104**, 8941–8946. (doi:10.1073/pnas.0702860104)
71. Aramwit P 2012 Flavinoids and carotenoids in silkworm cocoons. In *Silk: properties, production and uses* (ed. P Aramwit), pp. 87–97. New York, NY: Nova Science Publishers.
72. Dong Y, Dai F, Ren Y, Hui L, Yang P, Liu Y, Li X, Wang W, Hui X. 2015 Comparative transcriptome analyses on silk glands of six silkmoths imply the genetic basis of silk structure and coloration. *BMC Genomics* **16**, 203. (doi:10.1186/s12864-015-1420-9)
73. Toews DPL, Hofmeister NR, Taylor SA. 2017 The evolution and genetics of carotenoid processing in animals. *Trends Genet.* **33**, 171–182. (doi:10.1016/j.tig.2017.01.002)
74. Rimington C, Kennedy GY 1962 Porphyrins: structure, distribution, and metabolism. In *A comprehensive treatise. Vol. IV. Constituents of life-part B* (eds M Florkin, HS Mason), pp. 558–614. New York, NY: Academic Press.
75. Yazawa K, Masunaga H, Hikima T, Numata K. 2016 Influence of water content on the β-sheet formation, thermal stability, water removal, and mechanical properties of silk materials. *Biomacromolecules* **17**, 1057–1066. (doi:10.1021/acs.biomac.5b01685)
76. Plaza GR, Guinea GV, Perez-Riguiero J, Elices M. 2006 Thermo-hygro-mechanical behavior of spider dragline silk: glassy and rubbery states. *J. Polym. Sci.* **44**, 994–999. (doi:10.1002/polb.20751)
77. Guan J, Porter D, Vollrath F. 2013 Thermally induced changes in dynamic mechanical properties of native silks. *Biomacromolecules* **14**, 930–937. (doi:10.1021/bm400012k)